Graph-Based Analysis of Brain Connectivity in Major Depressive Disorder Using Electroencephalography

A. Jahanian Najafabadi[1,2] and K. Bagh[3]

1. Dept. Cognitive Neuroscience, Bielefeld University, Bielefeld, Germany
2. School of Business, Social and Decision Sciences, Constructor University Bremen, Bremen, Germany
3. Dept. of Technology, Bielefeld University, Bielefeld, Germany
amir.jahanian@uni-bielefeld.de, khaled.bagh@uni-bielefeld.de

***Abstract*— In line with our prior research, we aimed to identify and classify biomarkers of major depressive disorder (MDD) using electroencephalography (EEG) in patients and age-matched healthy children and adolescents. To achieve this, resting-state eyes-closed EEG data were pre-processed, and the analysis was performed on a channel-wise and Regions of Interest (ROI)-wise basis. We computed several resting-state Functional Connectivity (rsFC) measurements using a Multivariate Auto-Regressive (MVAR) model. The resulting connectivity measurements were then used to train a Random Forest model. We analyzed the best-performing models to understand the model's decision-making process and identify the learned biomarkers. Overall, the Random Forest model achieved a F1-score of 0.975 and a Matthews Correlation Coefficient (MCC) of 0.970. The model's test scores were highest with Partial Directed Coherence (PDC) and its variants. Additionally, we found that direct measurements, specifically PDC Factor and direct Directed Transfer Function (dDTF), performed better than other variants.**

Keywords*— *Electroencephalography, Children, Adolescents, Major Depressive Disorder, Graph Convolutional Network

I. Introduction

Numerous machine learning and deep learning algorithms have been employed in previous studies to develop diagnostic models for the early detection of Major Depressive Disorder (MDD), one of the most common psychiatric disorders. MDD is a heterogeneous condition that affects individuals from childhood through old age [1]. The high prevalence of MDD worldwide underscores the need for the scientific community to enhance early diagnosis and improve treatment processes. Although many studies have been conducted, the specifics of how brain connectivity within different regions is altered at the level of neuronal oscillations remain largely unclear. Addressing this challenge effectively requires a multidisciplinary approach that integrates neuroscientific, psychological, and computational expertise to meet the needs of both researchers and clinicians. In this research, we utilize a graph-based network applied to resting-state EEG functional connectivity to investigate and deepen our understanding of the brain networks involved in MDD in children and adolescents. The graph-based networks are one of the most utilized graph-based deep learning models for modeling graph data structures, such as networks. This is due to the exceptional ability of graph-based approaches to manage intricate pairwise relationships in both imaging and non-imaging features among different subjects, allowing for more nuanced and comprehensive data analysis (Parisot et al., 2018[2]). Therefore, we aim to improve classification models for diagnosing MDD among children and adolescents by comparing them with healthy age-matched individuals. Unlike most studies that have used fMRI datasets, we focus on EEG data as a non-invasive and recommended method to measure brain functional activities. This approach helps us deepen our understanding of MDD compared to healthy brain connectivity networks, utilizing more accessible and cost-effective neuroimaging techniques, such as EEG [3].

II. Background

II-A. Graph-based Analysis of Resting-state Functional Connectivity in Major Depressive Disorder

Using a Graph-based Analysis approach, a recent study by Qin et al. revealed an accuracy of 81.5% (95%CI: 80.5-82.5%, AUC: 0.865) applied to the large resting-state functional MRI datasets. Their results classified fronto-parietal, and cingulo-opercular networks within the default mode network and further reported left inferior parietal area is associated with the severity of depression [4]. A study by Olbrich et al.(2014) [5] using rsFC demonstrated increased alpha and decreased beta as potential biomarkers for MDD. Alpha activities were observed in the subgenual prefrontal cortex and left dorsolateral and mediolateral prefrontal cortex. Decreased cortical connectivity in beta activities was also found between the subgenual prefrontal cortex and right dorsolateral and mediolateral prefrontal cortex in MDD patients. Another study by Li et al. using graph theory analysis obtained an accuracy of 80.74% for recognizing the abnormal organization of functional connectivity networks in mild depression in young adult participants aged 18-24 years. Their study revealed a lower clustering coefficient and a greater characteristic path length in the MDD group compared to the healthy group. Jin et al. [6] further reported an abnormal hyperactive amygdala in depressed adolescents; and reduced hippocampal volume leading to an atrophy of hippocampal neurons compared to the healthy group Lee et al., 2002 [7].

To our knowledge, despite numerous studies in this line of research, no clear and optimized model has been introduced by the scientific community to detect abnormal biomarkers and distinguish MDD from healthy individuals with the highest accuracy, especially in children and adolescents. Additionally, the lack of consistency in the literature, such as varying participant ages and sample sizes, motivated us to test a graph-based analysis approach to classify both normal and abnormal biomarkers, particularly MDD, among children and adolescents.

III. Metrial and methods

III-A. Dataset

This study involved 214 datasets of children and adolescents aged 5 to 21, with 44 diagnosed with MDD and 170 classified as healthy (labeled HBN). The data were obtained from the publicly available Healthy Brain Network (HBN) dataset [8]. Resting-state data under closed eyes conditions were chosen for this study, recorded at a sampling rate of 500 Hz and a bandpass of 0.1 to 100 Hz using a 128 Channel EEG HydroCel Geodesic system by Electrical Geodesics Inc. However, after processing and excluding outer channels, only 109 channels were retained. The EEG electrode distribution on the scalp is depicted in figure 1.

III-B. Pre-processing

The data pre-processing was divided into two main steps, EEG data pre-processing and connectivity model computation. The pipeline used is described in [9]. The EEG pre-processing involves using the prep pipeline [10] to detect bad channels, followed by interpolation of the bad channels. A bandpass filter (1-70 Hz) was applied, followed by a notch filter at 60 Hz to eliminate power line artifacts. The data was then resampled at 256 Hz and referenced based on channel average. Independent Component Analysis (ICA) was then applied to detect bad artifacts to be removed before further computations. The EEG data was segmented into chunks of 4000 samples (15.6 seconds), and then for each segment a single Multi-Variate Auto-Regressive Integrated Component Analysis (MVARICA) model [11] was fitted to the data. First, the model hyperparameters were optimized. To that end, the segmented EEG data were further epoched into single-second epochs (15.6 seconds produced 15 epochs). The model order parameter was optimized by minimizing the mean squared generalization error on the epoched data by leaving one out of cross-validations (LOOCV). The optimization process was done on model order between 1 and 20. The delta ridge penalty parameter was optimized through the bisection search method [12]. It should be noted that the optimization step was performed on all EEG chunks independently under the assumption that the EEG signal was non-stationary. The MVARICA model was then fitted to the original segmented EEG data [11]. Using the fitted model, it was possible to compute several connectivity measures [13]: from MVARICA. The noise covariance matrix and the model coefficients were extracted to compute the Coherence [14], Partial Coherence [15], PDC [16], full frequency PDC (ffPDC) [17], PDC factor [16], generalized PDC (gPDC) [18], Direct Transfer Function (DTF) [19], full frequency DTF (ffDTF) [20], dDTF [20], and generalized DTF (gDTF) [21] between all channels in both directions.

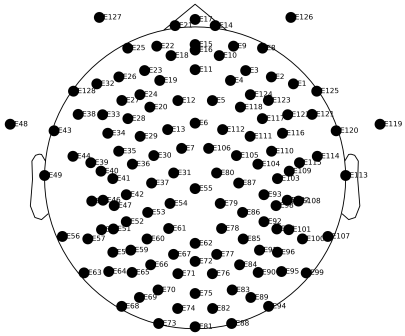

Figure 1. Channel location of 128 channels in the HBN dataset

Coherence is a measure of the statistical dependencies between different signals, while **Partial Coherence** evaluates the linear time-invariant relationship between two signals. Both Coherence and Partial Coherence measure the strength of the connection between two signals; however, Partial Coherence is better suited for isolating the effects of other channels and noise. **PDC** is a measure used to determine if two signals are significantly correlated (coherent). It also relies on the Granger causality principle to introduce a direction that governs these interactions, indicating which channel or brain area influences other channels or areas. **ffPDC** and **gPDC** are different versions of PDC, where ffPDC is normalized across all frequency bands, unlike PDC, which is normalized for each frequency band. gPDC is a scale-invariant version of PDC immune to static gain [22]. **PDC Factor** is similar to the PDC measure, but it focuses on direct interactions between the channels ignoring any indirect interaction. **DTF** is derived from the transfer function of the associated MVAR model, where DTF would estimate the flow of information from one channel to another, it mainly assesses how electrical activity from one channel influences another channel, where it mainly considers the amplitude and phase shift of the two signals. **ffDTF**, **dDTF** and **gDTF** are modified versions of DTF, where ffDTF is normalized across the full frequency band instead of each one as in DTF, dDTF provides more direct measures, where it ignores indirect channels relationship through a middle channel, removing indirect influence between any two

channels, and gDTF provides a more robust scale-invariant measurement.

It should be noted that all measurements were computed with a frequency resolution of 2500 samples between 0 and half the sampling rate (0-128 Hz). The measurements were then split according to the frequency ranges **Delta: 1-4 Hz, Theta: 4-8 Hz, Alpha: 8-12, Beta: 12-30, and Gamma: 30-70 Hz**. The connectivity measurements were averaged across channels to form the connectivity measurements for the ROI.

III-C. Random Forest

A Random Forest classifier is employed [23], utilizing an ensemble learning approach. Random Forest builds a forest of decision trees, where each tree is trained on a subset of the data. Then, the trees collectively vote on the majority class for classification. In this study, a Random Forest model was imported from the Python scikit-learn library with 20 estimators (a.k.a. random trees). Entropy was chosen as the criterion to measure the quality of data splits, and the random state was set to 7 for reproducibility. Class weights were also applied to address the class imbalance, as per the equation [1].

III-D. Model training

During model training, the input data is structured in tabular form, with rows representing samples from segmented participant data across each frequency band. The dataset comprises 31,290 rows in total, consisting of 4,995 samples from individuals with MDD and 26,295 from typically developing individuals (HBN). Columns represent attributes, which include connectivity measurements either channel-wise (11,881 attributes per measurement) or ROI-wise (49 attributes per measurement). An additional column specifies the frequency band corresponding to each connectivity measurement. Each model was trained separately on every individual connectivity measurement, except for Coherence and Partial Coherence. These two measurements included both real and imaginary values, necessitating separate columns for these components. Specifically, Random Forest models were trained on the pure real values of Coherence and Partial Coherence and real and imaginary values separately. The Random Forest model utilized 5-fold cross-validation, with data split subject-wise, with the metrics recorded being **F1-Score**, **Specificity**, **Cohen Kappa**, **MCC**. The best model was selected based on the highest F1-Score observed across each fold.

The **F1 score**, which ranges from 0 to 1, measures a model's accuracy, particularly valuable in imbalanced data scenarios. A good F1 score exceeds 0.7, indicating high precision and recall. **Cohen Kappa** is a statistic assessing the inter-rater reliability for categorical items. It considers the possibility of agreement occurring by chance in classification. Scores range from 0 to 1, with 0.6-0.8 considered good and scores above 0.8 very good. **MCC** is widely used in machine learning to evaluate binary classification quality, especially in imbalanced data contexts. It ranges from -1 to 1, with scores greater than ∓ 0.3 being moderate and scores larger than ∓ 0.5 being strong.

IV. Visualization of EEG-Based Brain Network Patterns

Seven ROIs are identified and illustrated in Figure 2 to distinguish important channels or ROIs between MDD and HBN. The model employs a method to rank the importance of attributes in each dataset. Random Forest inherently ranks features by assessing the importance of each attribute in predicting accuracy.

V. Experimental results

V-A. Setup

Before initiating training, weights were added to each class to account for the class imbalance. The weights were calculated in each fold according to equation [1].

$$W_j = \frac{n_{samples}}{n_{classes} * n_{jsamples}} \tag{1}$$

W_j is the weight of class j, $n_{samples}$ is the total number of samples used for training, $n_{classes}$ is the total number of classes, and $n_{jsamples}$ is the number of training samples belonging to class j. Additionally, the training of the models was done in Python 3.10.12, MNE 1.4.2, scot 0.2.1, Tensorflow 2.12.0, Keras 2.12.0, dask 2022.12.1, scipy 1.10.1, and numpy 1.22.4, scikit-learn 1.3.2.

V-B. Results

Training results are presented in Table 1, showing Random Forest test outcomes on a channel-wise basis. Notably, the Random Forest model achieved its highest F1-Score of 0.975 with PDC Factor, accompanied by a Specificity of 0.999, MCC of 0.970, and Cohen's Kappa score of 0.969. PDC and all its related measurements consistently scored greater than 0.9 across

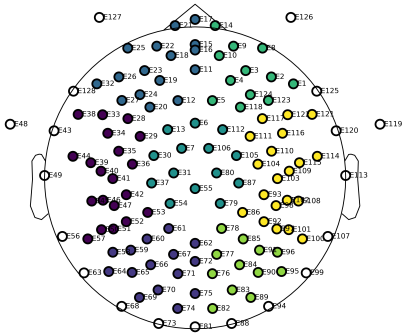

Figure 2. Region Of Interest (ROI)

all metrics. Random Forest performed better with PDC and its related measurements compared to DTF and its variants. It is also notable that dDTF and PDC Factor, which disregards indirect channel influences, outperformed DTF and PDC and their other variants, which do account for such influences. The Random Forest also failed to effectively learn from Coherence and Real Coherence data, while managing to learn from Partial Coherence and Real Partial Coherence. Notably, Random Forest performed better with Coherence and Partial Coherence when imaginary values were excluded from consideration.

Table 1. Random Forest testing score in each connectivity measurement, channelwise

Frequency	F1 Scores	Specificity	MCC	Cohen Kappa
COH	0.451	0.998	0.491	0.395
Real COH	0.481	0.998	0.512	0.423
PC	0.892	0.999	0.876	0.869
Real PC	0.921	0.999	0.907	0.903
PDC	0.954	0.999	0.945	0.943
PDC Factor	0.975	0.999	0.970	0.969
ffPDC	0.964	0.999	0.956	0.955
gPDC	0.942	0.999	0.930	0.928
DTF	0.836	0.997	0.816	0.802
ffDTF	0.819	0.994	0.796	0.782
dDTF	0.848	0.996	0.827	0.816
gDTF	0.813	0.997	0.793	0.776

Examining the results from Table 2, it is notable that Random Forest test scores on ROI-wise basis show a decrease compared to channel-wise test scores. The Random Forest model with PDC Factor remains the top performer, achieving a F1 Score of 0.878, Specificity of 0.994, MCC of 0.857, and Cohen's Kappa of 0.851. PDC and its related measurements continue to outperform others, albeit with a slight drop of around 0.1 in F1 Score. In contrast, DTF and its related measurements show a more significant decrease, averaging 0.2 in F1 Score. Coherence fails to achieve classification, while Partial Coherence experiences an approximate 0.4 drop in F1 Score.

Table 2. Random Forest testing score in each connectivity measurement, ROI-wise

Frequency	F1 Scores	Specificity	MCC	Cohen Kappa
COH	0.089	0.997	0.160	0.068
Real COH	0.083	0.995	0.142	0.060
PC	0.491	0.998	0.522	0.434
Real PC	0.562	0.996	0.572	0.503
PDC	0.843	0.991	0.818	0.810
PDC Factor	0.878	0.994	0.857	0.851
ffPDC	0.858	0.994	0.835	0.827
gPDC	0.857	0.993	0.834	0.826
DTF	0.669	0.984	0.640	0.610
ffDTF	0.619	0.983	0.591	0.556
dDTF	0.627	0.985	0.602	0.566
gDTF	0.641	0.983	0.613	0.580

(a) PDC Factor

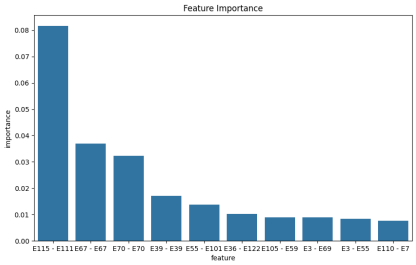

(b) ffPDC

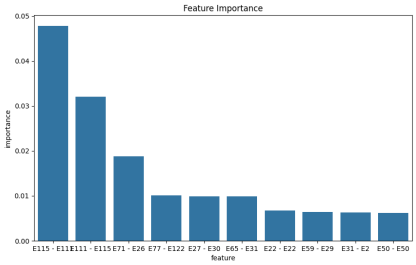

(c) dDTF

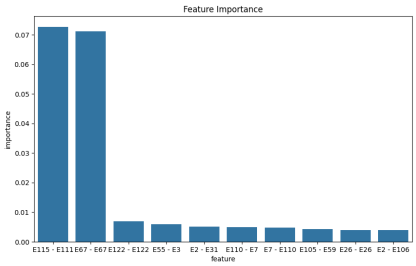

Figure 3. Learned feature importance from Random Forest Classifier, channel-wise

Looking at figure 3, the learned important features are depicted channel-wise for PDC Factor, ffPDC, and dDTF. Across all three measurements, it is noteworthy that the interaction between E115 and E111 emerges as the most important feature. Additionally, PDC Factor highlights interactions between E67-E67 and E70-E70, while ffPDC emphasizes E111-E115 and E71-E26. dDTF also identifies E67-E67 as a significant interaction. On the other hand, looking at figure 4, the ROI-wise feature importance is presented for PDC Factor, ffPDC, and dDTF. From table 2, it can be deduced that only the learned important features of PDC Factor and ffPDC are to be trusted, where the model managed to learn and classify with high accuracy. PDC Factor highlights interactions OR-OR, TR-TR, OL-OL, OL-FL, FL-FL, OL-FR, OR-FL, TL-TL, Center-Center and FR-FR. While ffPDC highlights OL-FL, FL-Center,

TR-TR, OR-FR, FL-OR, FL-OL, OR-FL, TL-OR, FR-FR, TR-FL.

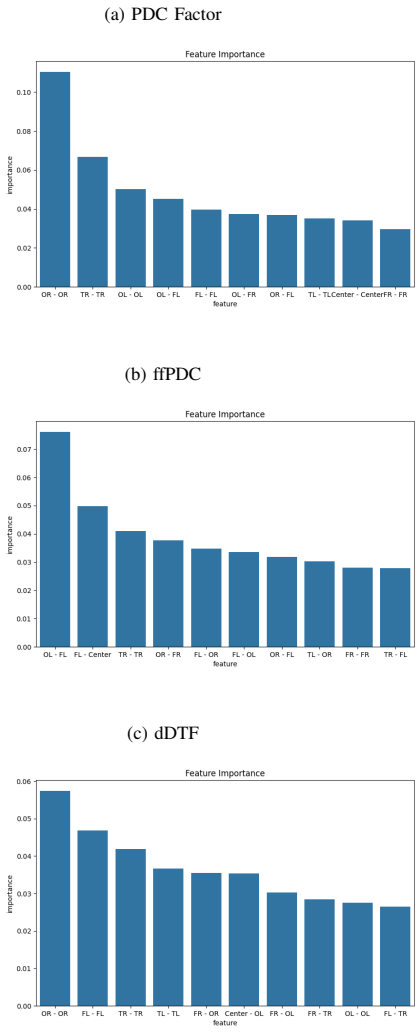

Figure 4. Learned feature importance from Random Forest Classifier, ROI-wise

Figure 5 shows the learned important interactions for PDC Factor, ffPDC, and dDTF, for inter-ROI interaction, excluding intra-ROI interactions. From table 2, dDTF will be excluded from further analysis. PDC Factor highlights two important interactions, OL-FL and OL-FR in both directions. With medium importance being placed on OL-OR, FL-TR, and FL-FR in both directions. While ffPDC highlights OL-FL and FL-Center in both directions, with medium importance placed on TL-OR, FL-OR, and TL-OL in both directions.

V-C. Discussion

In this research, we aimed to propose a diagnostic model using a graph-based network, particularly focusing on Random Forest, for classifying MDD using high-density

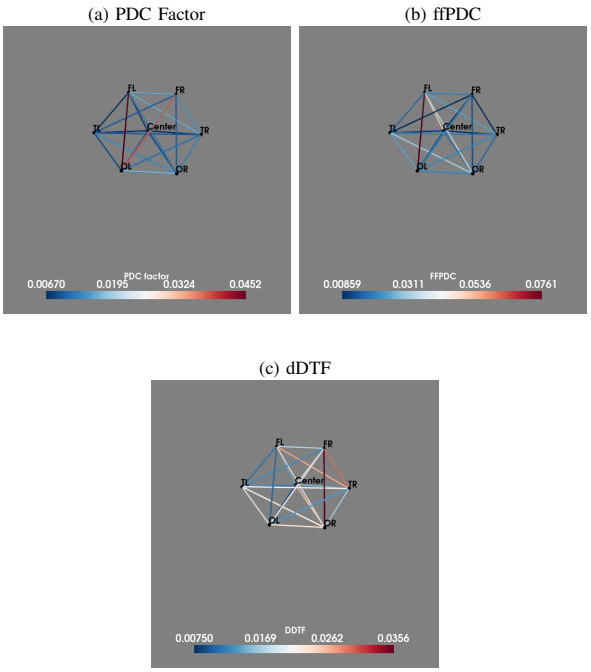

Figure 5. Inter-ROI map of most important features interactions detected by the Random Forest model

EEG as biomarkers compared to healthy children and adolescents. Our model achieved high classification scores: F1-Score of 0.975, Specificity of 0.999, MCC of 0.970, and Cohen's Kappa score of 0.969 for PDC Factor. In contrast, DTF and related measurements performed worse than PDC and its variants, which may be due to limitations in data availability during the construction of the MVARICA model. Adjusting the segmentation threshold might improve DTF and related measurements while maintaining adequate training data for the models.

Notably, measurements that exclude indirect influences performed better than others. This phenomenon can be attributed to the nature of of direct measurements and graph based models, where direct measurements capture causal interactions more explicitly, an environment where these causal interactions are captured is where graph based model excel, as discussed in [24].

In conclusion, we recommend replicating this study to validate our findings. Furthermore, future research should explore direct measurements with graph models, considering a larger segmentation threshold to enhance the evaluation of DTF and its related measurements, particularly dDTF.

VI. Conclusions

We conclude our findings drawn from extensive high-density clinical EEG datasets demonstrate the feasibility and effectiveness of employing graph networks to characterize MDD. These results underscore the potential of graph networks in advancing our understanding of the neurophysiology of MDD by pinpointing clinically significant disruptions in functional networks.

Acknowledgments

This manuscript was prepared using limited access to datasets obtained from the USA BioBank provided by the Child Mind Institute (CMI), Healthy Brain Network. The views expressed in this manuscript are those of the authors and do not necessarily reflect the opinions or views of the CMI. EEG datasets were credited by CMI to Dr. Amir Jahanian Najafabadi under an official agreement signed by Constructor University Bremen (formerly known as Jacobs University Bremen), for which we are grateful.

References

[1] K. V. Athira, S. Bandopadhyay, P. K. Samudrala, V. Naidu, M. Lahkar, and S. Chakravarty, "An overview of the heterogeneity of major depressive disorder: current knowledge and future prospective," *Current neuropharmacology*, vol. 18, no. 3, pp. 168–187, 2020.

[2] S. Parisot, S. I. Ktena, E. Ferrante, M. Lee, R. Guerrero, B. Glocker, and D. Rueckert, "Disease prediction using graph convolutional networks: application to autism spectrum disorder and alzheimer's disease," *Medical image analysis*, vol. 48, pp. 117–130, 2018.

[3] Y. Noda, K. Sakaue, M. Wada, M. Takano, and S. Nakajima, "Development of artificial intelligence for determining major depressive disorder based on resting-state eeg and single-pulse transcranial magnetic stimulation-evoked eeg indices," *Journal of Personalized Medicine*, vol. 14, no. 1, p. 101, 2024.

[4] K. Qin, D. Lei, W. H. Pinaya, N. Pan, W. Li, Z. Zhu, J. A. Sweeney, A. Mechelli, and Q. Gong, "Using graph convolutional network to characterize individuals with major depressive disorder across multiple imaging sites," *EBioMedicine*, vol. 78, 2022.

[5] S. Olbrich, A. Tränkner, T. Chittka, U. Hegerl, and P. Schönknecht, "Functional connectivity in major depression: increased phase synchronization between frontal cortical eeg-source estimates," *Psychiatry Research: Neuroimaging*, vol. 222, no. 1-2, pp. 91–99, 2014.

[6] C. Jin, C. Gao, C. Chen, S. Ma, R. Netra, Y. Wang, M. Zhang, and D. Li, "A preliminary study of the dysregulation of the resting networks in first-episode medication-naive adolescent depression," *Neuroscience letters*, vol. 503, no. 2, pp. 105–109, 2011.

[7] A. L. Lee, W. O. Ogle, and R. M. Sapolsky, "Stress and depression: possible links to neuron death in the hippocampus," *Bipolar disorders*, vol. 4, no. 2, pp. 117–128, 2002.

[8] L. M. Alexander, J. Escalera, L. Ai, C. Andreotti, K. Febre, A. Mangone, N. Vega-Potler, N. Langer, A. Alexander, M. Kovacs *et al.*, "An open resource for transdiagnostic research in pediatric mental health and learning disorders," *Scientific data*, vol. 4, no. 1, pp. 1–26, 2017.

[9] A. Jahanian Najafabadi and K. Bagh, "From power to connectivity: A comprehensive eeg analysis approach in python," Under review.

[10] N. Bigdely-Shamlo, T. Mullen, C. Kothe, K.-M. Su, and K. A. Robbins, "The prep pipeline: standardized preprocessing for large-scale eeg analysis," *Frontiers in neuroinformatics*, vol. 9, p. 16, 2015.

[11] G. Gómez-Herrero, M. Atienza, K. Egiazarian, and J. L. Cantero, "Measuring directional coupling between eeg sources," *Neuroimage*, vol. 43, no. 3, pp. 497–508, 2008.

[12] M. A. van de Wiel, M. M. van Nee, and A. Rauschenberger, "Fast cross-validation for multi-penalty high-dimensional ridge regression," *Journal of Computational and Graphical Statistics*, vol. 30, no. 4, pp. 835–847, 2021.

[13] M. Billinger, C. Brunner, and G. R. Müller-Putz, "Single-trial connectivity estimation for classification of motor imagery data," *Journal of neural engineering*, vol. 10, no. 4, p. 046006, 2013.

[14] P. L. Nunez, R. Srinivasan, A. F. Westdorp, R. S. Wijesinghe, D. M. Tucker, R. B. Silberstein, and P. J. Cadusch, "Eeg coherency: I: statistics, reference electrode, volume conduction, laplacians, cortical imaging, and interpretation at multiple scales," *Electroencephalography and clinical neurophysiology*, vol. 103, no. 5, pp. 499–515, 1997.

[15] P. J. Franaszczuk, K. J. Blinowska, and M. Kowalczyk, "The application of parametric multichannel spectral estimates in the study of electrical brain activity," *Biological cybernetics*, vol. 51, pp. 239–247, 1985.

[16] L. A. Baccalá and K. Sameshima, "Partial directed coherence: a new concept in neural structure determination," *Biological cybernetics*, vol. 84, no. 6, pp. 463–474, 2001.

[17] M. Billinger, C. Brunner, and G. R. Müller-Putz, "Scot: a python toolbox for eeg source connectivity," *Frontiers in neuroinformatics*, vol. 8, p. 22, 2014.

[18] L. Faes, S. Erla, and G. Nollo, "Measuring connectivity in linear multivariate processes: definitions, interpretation, and practical analysis," *Computational and mathematical methods in medicine*, vol. 2012, no. 1, p. 140513, 2012.

[19] M. J. Kaminski and K. J. Blinowska, "A new method of the description of the information flow in the brain structures," *Biological cybernetics*, vol. 65, no. 3, pp. 203–210, 1991.

[20] A. Korzeniewska, M. Mańczak, M. Kamiński, K. J. Blinowska, and S. Kasicki, "Determination of information flow direction among brain structures by a modified directed transfer function (ddtf) method," *Journal of neuroscience methods*, vol. 125, no. 1-2, pp. 195–207, 2003.

[21] L. Faes, S. Erla, and G. Nollo, "Measuring connectivity in linear multivariate processes: definitions, interpretation, and practical analysis," *Computational and mathematical methods in medicine*, vol. 2012, no. 1, p. 140513, 2012.

[22] G. Chiarion, L. Sparacino, Y. Antonacci, L. Faes, and L. Mesin, "Connectivity analysis in eeg data: a tutorial review of the state of the art and emerging trends," *Bioengineering*, vol. 10, no. 3, p. 372, 2023.

[23] S. J. Rigatti, "Random forest," *Journal of Insurance Medicine*, vol. 47, no. 1, pp. 31–39, 2017.

[24] L. Q. Tay, "Rethinking graphical causal models," *Nature Reviews Psychology*, vol. 1, no. 8, pp. 438–438, 2022.